UC Davis
UC Davis Previously Published Works

Title

Deleting a UBE3A substrate rescues impaired hippocampal physiology and learning in Angelman syndrome mice

Permalink

https://escholarship.org/uc/item/6972t7p2

Journal

Scientific Reports, 11(1)

ISSN

2045-2322

Authors

Sell, Gabrielle L
Xin, Wendy
Cook, Emily K
et al.

Publication Date

2021

DOI

10.1038/s41598-021-97898-w

Peer reviewed

scientific reports

OPEN

Deleting a UBE3A substrate rescues impaired hippocampal physiology and learning in Angelman syndrome mice

Gabrielle L. Sell[1,2,5,9]✉, Wendy Xin[2,3,6,9], Emily K. Cook[1,9], Mark A. Zbinden[1,7], Thomas B. Schaffer[1,8], Robert N. O'Meally[1,4], Robert N. Cole[1,4] & Seth S. Margolis[1,2]✉

In humans, loss-of-function mutations in the *UBE3A* gene lead to the neurodevelopmental disorder Angelman syndrome (AS). AS patients have severe impairments in speech, learning and memory, and motor coordination, for which there is currently no treatment. In addition, *UBE3A* is duplicated in >1–2% of patients with autism spectrum disorders—a further indication of the significant role it plays in brain development. Altered expression of UBE3A, an E3 ubiquitin ligase, is hypothesized to lead to impaired levels of its target proteins, but identifying the contribution of individual UBE3A targets to UBE3A-dependent deficits remains of critical importance. Ephexin5 is a putative UBE3A substrate that has restricted expression early in development, regulates synapse formation during hippocampal development, and is abnormally elevated in AS mice, modeled by maternally-derived *Ube3a* gene deletion. Here, we report that Ephexin5 can be directly ubiquitylated by UBE3A. Furthermore, removing Ephexin5 from AS mice specifically rescued hippocampus-dependent behaviors, CA1 physiology, and deficits in dendritic spine number. Our findings identify Ephexin5 as a key driver of hippocampal dysfunction and related behavioral deficits in AS mouse models. These results demonstrate the exciting potential of targeting Ephexin5, and possibly other UBE3A substrates, to improve symptoms of AS and other UBE3A-related developmental disorders.

Angelman syndrome (AS) is a neurodevelopmental disorder that affects approximately one in 15,000 individuals and is characterized by severe motor dysfunction, loss of speech, frequent seizures, and debilitating cognitive impairments[1,2]. The majority of AS patients carry genomic lesions that disrupt the E3 ubiquitin ligase UBE3A[3]. In humans, the *UBE3A* gene resides within chromosomal region 15q11-13 and is subject to brain-specific genomic imprinting, with predominant transcription of the maternal allele in neuronal cells across the brain[4,5]. Inheritance of an abnormal, inactive maternal copy of the *UBE3A* gene is currently thought to account for 85–90% of AS cases[4]. Consistent with this, deletion of the maternal copy of UBE3A in mice (AS mice) leads to clear cellular, electrophysiological, and behavioral deficits in these animals[6].

UBE3A encodes a HECT (Homologous to the E6-AP Carboxyl Terminus) domain E3 ubiquitin ligase that catalyzes the addition of ubiquitin to lysine residues on substrate proteins. Several mutations identified in AS patients specifically disrupt this ubiquitin ligase activity of UBE3A while still expressing full-length protein[7]. UBE3A-dependent ubiquitylation is primarily thought to target substrates for degradation by the 26S proteasome[8]. Ubiquitin-dependent proteasome degradation clears unwanted proteins and is necessary to maintain proper intracellular protein homeostasis and neuronal function[9]. Thus, the possibility that aberrant levels

[1]Department of Biological Chemistry, The Johns Hopkins University School of Medicine, Wood Basic Science Building Room 517, 725 N. Wolfe St., Baltimore, MD 21205, USA. [2]Solomon H. Snyder Department of Neuroscience, The Johns Hopkins University School of Medicine, Baltimore, MD 21205, USA. [3]Intramural Research Program, National Institute on Drug Abuse, National Institutes of Health, Baltimore, MD 21224, USA. [4]Mass Spectrometry and Proteomics Facility, The Johns Hopkins University School of Medicine, Baltimore, MD 21205, USA. [5]Present address: Center for Neuroscience, University of California-Davis, One Shields Avenue, Davis, CA 95616, USA. [6]Present address: Department of Neurology and the Weill Institute for Neurosciences, University of California, San Francisco, San Francisco, CA 94158, USA. [7]Present address: Human Metabolome Technologies America, Inc., Boston, MA 02134, USA. [8]Present address: NextCure Inc., Beltsville, MD 20705, USA. [9]These authors contributed equally: Gabrielle L. Sell, Wendy Xin and Emily K. Cook. ✉email: glsell@ucdavis.edu; smargol7@jhmi.edu

1
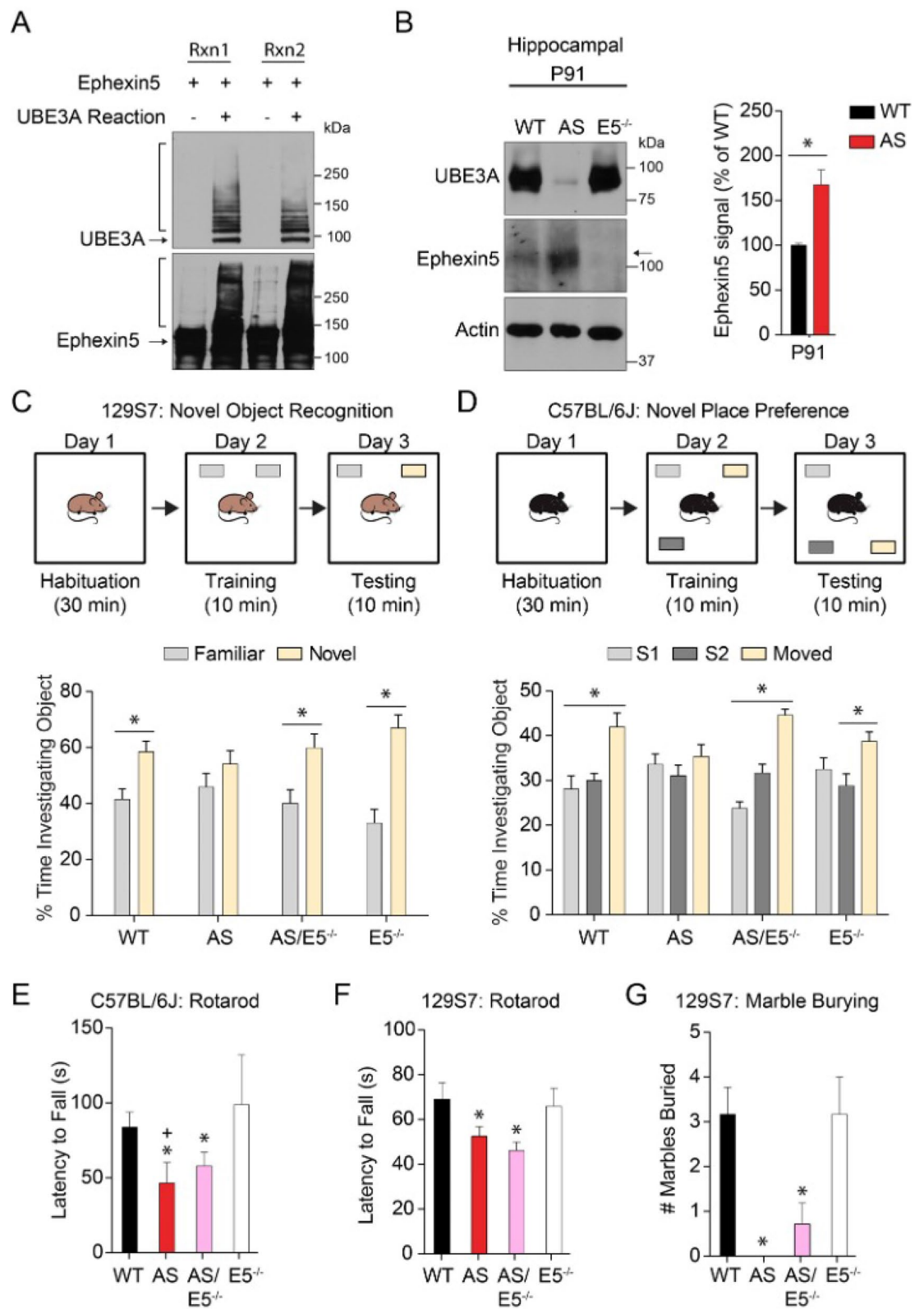
◄**Figure 1.** Ephexin5 is upregulated in AS mouse hippocampal tissue and removal of Ephexin5 modulates learning and memory behavioral task. (**A**) In vitro ubiquitylation assays were performed using purified Ephexin5 protein in the presence or absence of UBE3A reaction buffer (containing UBE1, UBE2L3, UBE3A, E6, Ubiquitin, and Mg-ATP), as indicated. Replicates shown using immunoblot analysis with indicated antibodies. The arrows indicate the unmodified protein and the bracket indicates the smearing due to ubiquitylation. (**B**) Ephexin5 expression levels are elevated in AS mouse hippocampus. Hippocampi were dissected from wild-type (WT) and AS mice at P91 and lysates were prepared for immunoblotting with indicated antibodies. Quantification of Ephexin5 signal is normalized to Actin signal and compared to WT. Arrow indicates Ephexin5 band. Data are presented as mean ± SEM (n = 4 for WT, n = 5 for AS). *$p < 0.05$ (unpaired Student's t-test). (**C**) Object investigation in the NOR test in 3 month old 129S7 mice. Shown is the percent time spent investigating each object. Data are presented as mean ± SEM. *$p < 0.05$ (two-way ANOVA) compared to familiar within genotype with *post-hoc* Holm-Sidak correction. (**D**) Object investigation in the NPP test in 3 month-old C57Bl/6J mice. Shown is the percent time spent investigating each object. Data are presented as mean ± SEM. *$p < 0.05$ (two-way ANOVA) compared to the stationary objects (S1 and S2) or as indicated with *post-hoc* Bonferroni multiple comparisons test. (**E**) Latency for C57Bl/6J mice to fall off the rotating rod, measured in seconds. Data are presented as mean ± SEM. *$p < 0.05$ compared to E5$^{-/-}$, $^+p < 0.05$ compared to WT (one-way ANOVA) with *post-hoc* Tukey's multiple comparisons test. (**F**) Latency for 129S7 mice to fall off the rotating rod, measured in seconds. Data are presented as mean ± SEM. *$p < 0.05$ (one-way ANOVA) compared to WT and E5$^{-/-}$ with *post-hoc* Tukey's multiple comparisons test. (**G**) Number of marbles buried or covered 2/3 in 20 min by 129S7 mice. Data are presented as mean ± SEM. *$p < 0.05$ compared to WT and E5$^{-/-}$ (one-way ANOVA) with *post-hoc* Tukey's multiple comparisons test. See also Supplementary Fig. 1. Sample size (n) reported in Materials and Methods. Degrees of freedom and exact p values are reported in Supplementary Table 2 and Supplementary Table 3. Behavior analysis used ODlog (v 2.5 http://www.macropodsoftware.com/odlog/).

of UBE3A targets are causing the numerous phenotypic deficits observed in AS is a prevailing hypothesis in the AS field. This hypothesis has generated excitement among AS researchers as it could lead to the development of therapeutic strategies targeting specific UBE3A substrates. Currently, however, the involvement of direct UBE3A substrates in AS phenotypes remains largely untested, although manipulation of PTPA, a new putative substrate, has shown ameliorative effects[10].

UBE3A is highly expressed in the hippocampus, a brain region that is critical for learning and memory[11]. Ephexin5, a RhoA guanine nucleotide exchange factor, is a candidate UBE3A substrate that is also enriched in the hippocampus. During development, Ephexin5 acts as a brake on excitatory synapse formation[12]. Previous work identified Ephexin5 as a probable substrate of the ubiquitin–proteasome system and reported a decrease in total ubiquitylated Ephexin5 in AS mice[12]. Based on these data, we hypothesized that Ephexin5 is a direct substrate of UBE3A and that in AS mice, increased expression of Ephexin5 would be critically involved in UBE3A-dependent hippocampal dysfunction. Here we report that Ephexin5 can be directly ubiquitylated by UBE3A and is elevated in adult AS mice brains. Importantly, removal of Ephexin5 rescued hippocampus-related impairments in behavior, spine density, and electrophysiology in the CA1 region of AS mice. These data demonstrate the role of a UBE3A substrate in AS cognitive pathology and pinpoints Ephexin5 as a promising target for treating cognitive deficits in AS.

Results

Ephexin5 is ubiquitylated by UBE3A in vitro and Ephexin5 expression is increased in vivo in the hippocampus of AS mouse models.

Previous reports have demonstrated that Ephexin5 is ubiquitylated in brains of mice, which is, in part, dependent on the presence of UBE3A[12]. To determine whether Ephexin5 can be directly ubiquitylated by UBE3A, we used purified Ephexin5 protein and incubated it in an in vitro purified UBE3A ubiquitin ligase assay. Samples were then run on SDS-PAGE for immunoblot analysis using antibodies raised against Ephexin5. We noted a shift in Ephexin5 mobility consistent with ubiquitin modification (Fig. 1A), which was dependent upon the presence of ATP and UBE3A (Supplementary Fig. 1A). E6 protein was included in the initial experiment to get enhanced ubiquitylation of Ephexin5 since it has previously been described to stimulate UBE3A activity at least toward other substrates such as p53[13,14]. Recombinant E6 protein used in this study is type 16 (UniProt # P03126, see Supplementary Table 1) which is an oncoprotein encoded by the Human Papillomavirus. E6 is intimately associated with the events that result in the malignant conversion of virally infected cells.

While E6 protein enhances this in vitro assay, it is not required for UBE3A to ubiquitylate Ephexin5 at several residues (Supplementary Fig. 1A). We also noted that in the presence of E6, UBE3A was more efficiently auto-ubiquitylated (Supplementary Fig. 1A). We confirmed that Ephexin5 was being directly ubiquitylated by using mass spectrometry analysis. Through this analysis we were able to identify ubiquitylation sites on Ephexin5 in the presence of UBE3A with and without E6 (Supplementary Fig. 1B,C). Taken together, based on these data Ephexin5 can be ubiquitylated by UBE3A. Consistent with the idea that this ubiquitylation targets Ephexin5 for proteasome degradation, previous findings have shown that Ephexin5 expression is elevated early in postnatal AS mouse brain[12]. To determine whether Ephexin5 levels were also elevated in adult hippocampus, when hippocampal-dependent behaviors and hippocampal synaptic transmission are known to occur, we measured hippocampal Ephexin5 levels in wild type (WT) and AS littermates of the 129S7 strain at postnatal day 91 (P91). Dissected hippocampi were lysed and prepared for SDS-PAGE and western analysis using antibodies raised against UBE3A, Ephexin5, or Actin. We detected a significant elevation in Ephexin5 antibody signal in AS mice as compared to WT littermate controls at this age (Fig. 1B).

Figure 2. *Ube3A^{loxp+}/camkIIa-cre^+* mice have increased Ephexin5 expression in the hippocampus and Ephexin5 ▶ dependent deficits in NPP. (**A**) 8 week old TdTomato cre reporter-positive, *camkIIa-cre^+* tissue was stained for TdTomato (red) with Hoechst (DAPI -blue) for nuclei labeling. On the left is a 10× image of one coronal section indicating strong hippocampal and some cortical expression. On the right are images of DG and CA1, indicating nearly 100% recombination in the excitatory cell layers. Scale bar = 10 μm (**B**) Ephexin5 expression levels are elevated in hippocampus from *ube3A^{loxp+}/camkIIa-cre^+* mice. Quantification of Ephexin5 and UBE3A signal is normalized to Actin signal and compared to *ube3Aloxp^+/camkIIa-cre^-* controls. Arrow indicates Ephexin5 band. Data are presented as mean ± SEM (n = 6 for *ube3A^{loxp+}/camkIIa-cre^+*, n = 5 for *ube3A^{loxp+}/camkIIa-cre^-*). * $p < 0.05$ (unpaired Student's t-test). (**C**) Latency for WT C57Bl/6J mice, with or without *camkIIa-cre* dependent *ube3A* removal, to fall off the rotating rod, measured in seconds. (**D**) Object investigation in the NPP test in 3 month-old C57Bl/6J mice, with or without *camkIIa-cre* dependent *ube3A* removal in a WT or E5^{−/−} background. Shown is the percent time spent investigating each object. Data are presented as mean ± SEM. *$p < 0.05$ (two-way ANOVA) compared to the stationary objects (S1 and S2) with *post-hoc* Bonferroni multiple comparisons test. See also Supplementary Fig. 2. Sample size (n) reported in Materials and Methods. Degrees of freedom and exact *p* values are reported in Supplementary Table 2 and Supplementary Table 3. Behavior analysis used ODlog (v 2.5 http://www.macropodsoftware.com/odlog/).

Removal of Ephexin5 in the AS mouse model rescues hippocampus-dependent behaviors.

To determine whether elevated levels of Ephexin5 play a crucial role in AS-relevant phenotypes, we used genetic approaches to delete Ephexin5 in the 129S7 AS mouse model. Breeding strategies were devised to generate wild type (WT), Angelman Syndrome (*Ube3A^{m-/p+}*, AS), Ephexin5 knockout (*Ephexin5^{−/−}*, E5^{−/−}) and double knockout (*Ube3A^{m-/p+}/Ephexin5^{−/−}*, AS/E5^{−/−}). Ephexin5's role in the nervous system has been predominantly described in the hippocampus where its expression is enriched[12]. Therefore, we tested WT, AS, AS/E5^{−/−}, and E5^{−/−} littermates on several hippocampus-dependent and hippocampus-independent behavioral tasks[15]. We used a traditional novel object recognition task (NOR) and passive avoidance to investigate hippocampus-dependent behaviors. While the AS mouse showed a lack of preference for the novel object (Fig. 1C), there was no difference in the response of any genotype within the passive avoidance (Supplementary Fig. 1D). However, these passive avoidance results are difficult to interpret, as none of the animals entered the dark arena on test day within the 5-min test trial. Importantly, removal of Ephexin5 in the AS mouse model was sufficient to restore preference for the novel object (Fig. 1C).

Previous studies indicate UBE3A deletion on pure 129S7 vs C57Bl/6J have different phenotype penetrance[16–18]. We sought to extend our observation in 129S7 strain into C57BL/6J to determine the general relevance of the Ephexin5 pathway in AS-associated hippocampal dependent phenotypes. We generated WT, AS, AS/E5^{−/−}, and E5^{−/−} littermates on C57Bl/6J. At P30, we noted a trending increase (*p* value > 0.07*) in* Ephexin5 levels in the AS mice (Supplementary Fig. 1E). We chose to test these mice in the novel place preference test (NPP) which our lab has extensive experience with[19] and is a similar task to NOR known to rely on the same brain area[20]. The AS animals did not prefer the moved object as measured by the amount of time spent investigating each object 24 h later, in contrast to the WT, AS/E5^{−/−}, and E5^{−/−} animals which showed a significant preference for the moved object (Fig. 1D). Interestingly, in the passive avoidance task, which requires both hippocampus and amygdala activity[21], Ephexin5 deletion did not rescue C57Bl/6J AS mouse behavior (Supplementary Fig. 1F).

In contrast to these more hippocampal specific learning tasks, Ephexin5 deletion did not improve AS mouse performance in the rotarod motor coordination task in either mouse strain (Fig. 1E,F) and the marble-burying task in the 129S7 strain[18] (Fig. 1G). This lack of rescue may be due to the regionally restricted expression and activity of Ephexin5, as neither the rotarod nor the marble-burying task is dependent on hippocampal function. However, it should be noted that our behavioral results align with previously reported phenotypes in the field[18,22–25]. These data provide evidence for regulation of hippocampal function by UBE3A in behaviorally relevant ways, which is at least in part dependent on the presence of Ephexin5. Moreover, we concluded that removal of Ephexin5 does not interfere with hippocampus-dependent learning or other behaviors in a wild-type background. Thus, removal of Ephexin5 appears to specifically rescue hippocampus-dependent learning deficits observed in AS mice, indicating that the elevation of Ephexin5 observed in AS mice may be pathological.

Conditional removal of UBE3A in excitatory forebrain neurons recapitulates learning and memory but not motor phenotypes of AS mice.

UBE3A is expressed throughout the nervous system in a variety of cell types, whereas Ephexin5 is most highly expressed in excitatory neurons within the hippocampus[12]. To determine whether UBE3A within hippocampal excitatory cells was responsible for the cognitive behavioral deficits observed in AS mice, we used the Cre/Lox system to conditionally remove UBE3A from the C57Bl/6J:ube3A^{loxp}[26]. In order to obtain robust, consistent recombination in CA1 and DG, we used the CamKIIa-Cre line, which is expressed in excitatory forebrain neurons by 2 weeks postnatally and produces robust recombination in hippocampus[27]. To identify the cells in which UBE3A expression was removed, we crossed the CamKIIa-Cre line with a TdTomato reporter line. At 8 weeks, expression of the reporter was detected in a subset of excitatory cortical neurons and robustly in the excitatory cell layers of CA1 and DG (Fig. 2A). Lysates from hippocampi of adult Cre^+ and Cre^- maternal Ube3A^{loxp+} were analyzed via Western blot for expression of UBE3A and Ephexin5. Compared to the hippocampi of Cre^- animals, in the hippocampi of Cre^+ animals UBE3A expression was significantly decreased, while Ephexin5 was significantly increased (Fig. 2B and Supplementary Fig. 2). Consistent with previous descriptions of Ephexin5 expression, in Cre^- animals expression of Ephexin5 in the cortex was undetectable as compared to hippocampus (Supplementary Fig. 2). Nevertheless, to determine whether the CamKIIa-Cre expression in a subset of cortical neurons produces deficits in cortex-dependent behaviors in UBE3a-Floxed mice, we tested animals on the rotarod task, which requires cortical
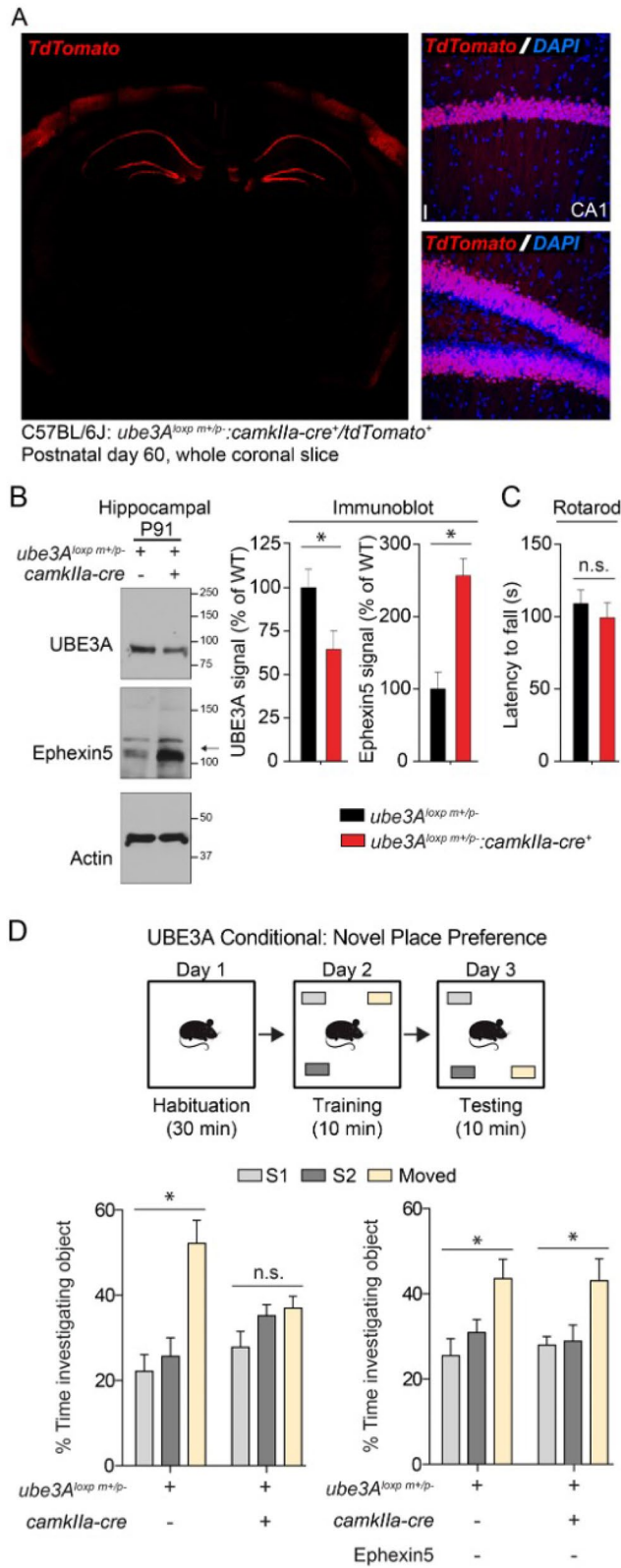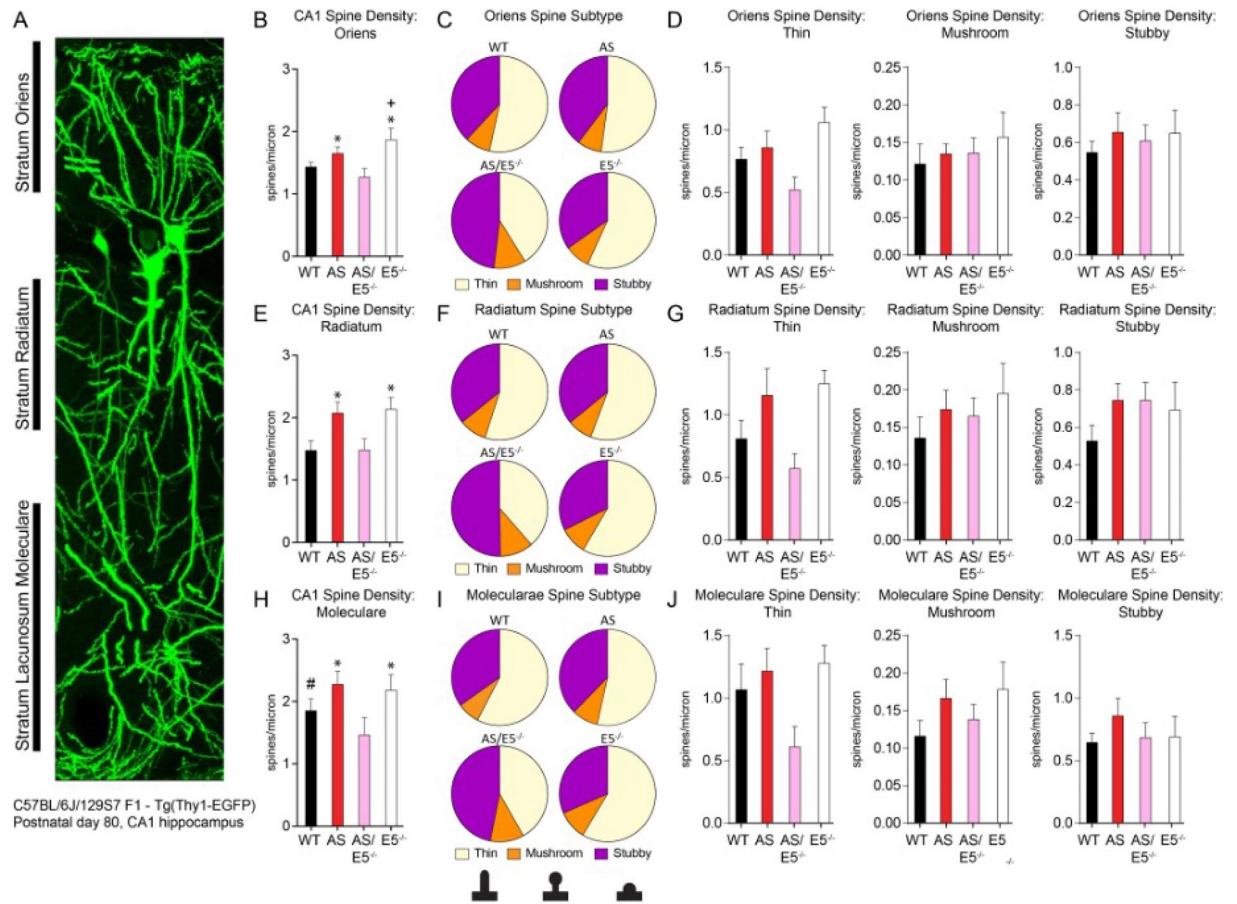
Figure 3. UBE3A expression in CA1 and location of spine analysis in CA1 GFP-positive neurons, related to Fig. 3. (**A**) Example CA1 GFP-positive neurons with the regions of interest labeled (stratum oriens, stratum radiatum, and stratum moleculare). Scale bar is 10 μm. (**B**) Oriens spine density in CA1. (**C**) Proportion of spine subtypes within WT, AS, AS/E5$^{-/-}$, and E5$^{-/-}$ oriens dendrites of CA1 neurons. (**D**) Spine density in the stratum oriens of CA1 neurons for thin, mushroom, and stubby morphologies. (**E**) Radiatum spine density in CA1. (**F**) Proportion of spine subtypes within WT, AS, AS/E5$^{-/-}$, and E5$^{-/-}$ radiatum dendrites of CA1 neurons. (**G**) Spine density in the stratum radiatum of CA1 neurons for thin, mushroom, and stubby morphologies. (**H**) Moleculare spine density in CA1. (**I**) Proportion of spine subtypes within WT, AS, AS/E5$^{-/-}$, and E5$^{-/-}$ moleculare dendrites of CA1 neurons. (**J**) Spine density in the stratum lacunosum moleculare of CA1 neurons for thin, mushroom, and stubby morphologies. One-way ANOVA, *post-hoc* Tukey's multiple comparisons test for panels B, E, and H. Two-way ANOVA, *post-hoc* Sidak's multiple comparisons test for panels D, G, and J. All data are presented as mean ± SEM (n = 3 for all genotypes) *$p < 0.05$ compared to WT and AS/E5$^{-/-}$, +$p < 0.05$ compared to AS, #$p < 0.05$ compared to AS/E5$^{-/-}$ for all panels. See also Supplementary Fig. 3. Degrees of freedom and exact *p* values are reported in Supplementary Table 2 and Supplementary Table 3. Image analysis was performed using Fiji/ImageJ (v2.0.0—imagej.nih.gov/ij/docs/guide/146–2.html), and NeuronStudio (research.mssm.edu/cnic/tools-ns.html).

function[28]. Expression of Cre in this subset of cortical neurons did not decrease the latency to fall from the rotating rod (Fig. 2C), as was measured in AS animals (Fig. 1E). In contrast, deficits in the novel place preference task were observed in Cre$^+$ animals (Fig. 2D), similar to the AS animals (Fig. 1C). Furthermore, this deficit was again rescued by removal of Ephexin5 (Fig. 2D), suggesting that Ephexin5 most likely acts within the hippocampus to ameliorate these deficits.

Removal of Ephexin5 restores hippocampal CA1 spine density in AS mice to WT levels. Previous studies in visual cortex and striatum have reported deficits in synaptic transmission in AS mice[29–31], as well as decreases in spine density in AS mice using Golgi staining or phalloidin staining in CA1[31,32]. We suspected that, since Ephexin5 is involved in developmental regulation of dendritic spine formation, AS mice may also have altered spine morphology in the hippocampus. Furthermore, novel object recognition and object location recall have been linked specifically to hippocampal CA1 function[20,33]. To test this idea, we included the Thy1-EGFP (enhanced green fluorescent protein expressed from the Thy1 promoter) line in our crosses that generate WT, AS, AS/E5$^{-/-}$ and E5$^{-/-}$ lines to label a subset of neurons in the hippocampus with EGFP. At 11 weeks of age, the Thy1-EGFP labeled lines were anesthetized and perfused. Brains were then sectioned and imaged to visualize labeled pyramidal neurons. We focused on the CA1 region of hippocampus, where UBE3A is highly expressed

(Supplementary Fig. 3A). We visualized dendritic spines on individual EGFP-expressing neurons using confocal microscopy (Supplementary Fig. 3B). Dendrites from each CA1 pyramidal neuron were imaged and spine densities quantified from the stratum radiatum (s.r.), stratum oriens (s.o.) and stratum lacunosum-molecular (s.l.m) (Fig. 3A,B,E,H). Changes in dendritic spine density were consistent across strata of imaged CA1 pyramidal neurons and thus combined in the analysis. Unexpectedly, blinded analysis revealed an increase in spine density on CA1 pyramidal neurons of AS mice. This is in contrast to a previous study which reported, using Golgi staining, decreased dendritic spine density in the CA1 of the AS hippocampus[32]. In our study, the relative abundance of spine types (stubby, thin, mushroom) did not differ significantly between AS and WT mice (Fig. 3C,D,F,G,I,J), however the changes between AS and AS/E5$^{-/-}$ animals is driven by reductions in thin spines. Given that thin spines are increased in AS mice in other studies[10], we believe our data indicates the "rescue" follows a similar mechanism of reducing this thin spine subtype. Thin spines are typically considered immature with smaller synapses and have increased capacity for plasticity (Bourne and Harris 2007). Therefore, it is possible this decrease in thin spines in the AS/E5$^{-/-}$ compared to the AS is a result of conversion of these thin spines to a more mature state, thus allowing for the rescue of behavioral phenotypes. Consistent with previous ex *vivo* studies in developing E5$^{-/-}$ animals[12,34], we observed ex vivo that dendrites from adult E5$^{-/-}$ animals also showed an increase in spine density compared to WT controls. Importantly, deletion of Ephexin5 in the AS/E5$^{-/-}$ mice restored dendritic spine density to WT levels. It is not surprising Ephexin5 manipulation contributes to UBE3A-dependent dendritic spine alterations, given that general manipulation of the cytoskeleton is able to rescue neuronal morphology better than UBE3A re-expression alone in vitro[35]. Our data has shown the removal of Ephexin5 has different repercussions on density and spine subtype composition depending on the presence of UBE3A, and indicates a complex interplay between dendritic spine morphology and UBE3A-dependent susceptibility.

Looking at the distribution of spine type, as measured by length and width of each dendritic spine counted, we observed that the proportions of spine subtypes from the AS/E5$^{-/-}$ mice were altered compared to other genotypes, with an increase in stubby spines and a decrease in thin spines (Fig. 3 and Supplementary Fig. 3). This change may be attributed to a consistent decrease in AS/E5$^{-/-}$ thin spines compared to AS and E5 animals. Stubby spines are most common in early postnatal development, after a loss of filopodia and before a large increase in thin and mushroom spines[36]. This decrease in thin spines may indicate that a larger subset of the spines in the AS/E5$^{-/-}$ animals are less mature or are developing later than spines in the other genotypes[37]. Taken together, these data identify a unique feature of AS mice, whereby in the CA1 there is an increase in dendritic spine density across strata compared to WT mice that is at least in part dependent on the presence of Ephexin5.

Removal of Ephexin5 restores CA1 excitatory transmission in AS mice to WT levels.

To determine the physiological consequence of the observed changes in dendritic spine density described in Fig. 3, we recorded miniature excitatory postsynaptic currents (mEPSCs) from pyramidal neurons in the CA1 (Fig. 4A). To measure number and strength of excitatory synapses in individual neurons, mEPSCs were isolated at -70 mV in the presence of tetrodotoxin (TTX, 1 µM), gabazine (1 µM), and APV (30 µM). Consistent with the observed increase in spine density, AS mice exhibited a higher frequency of mEPSCs than WT littermates (Fig. 4B); mEPSC amplitudes were not statistically different (Fig. 4C). Stimulus-evoked EPSCs were also significantly larger in AS mice (Supplementary Fig. 4A-B). This increase in excitatory inputs does not appear to result from a change in presynaptic glutamate release, as paired pulse ratios—a measure of presynaptic release probability—across a range of pulse intervals were not different between AS and WT mice (Supplementary Fig. 4C-D). Consistent with previous reports[12], E5$^{-/-}$ animals also exhibited higher mEPSC frequency relative to WT (Fig. 4B). However, mEPSC frequency did not differ between WT and AS/E5$^{-/-}$ mice (Fig. 4B). The average rise time and decay time of miniature events were slightly longer in AS/E5$^{-/-}$ mice, though not statistically different from WT (Fig. 4D–F). To determine whether evoked excitatory inputs were also similar between AS/E5$^{-/-}$ animals and WT animals, stimulus-evoked EPSCs were recorded from the CA1 of AS/E5$^{-/-}$ and WT littermate controls (Supplementary Fig. 4-E–F). In contrast to AS animals, AS/E5$^{-/-}$ animals exhibited only a slight decrease in EPSC amplitude at the highest stimulus intensity (Supplementary Fig. 4A-B), with no differences in paired pulse ratios (Supplementary Fig. 4G-H). Previous reports indicate that AS neurons are hyperexcitable and have an altered E/I balance[10,25,30,38] raising the possibility of a previously unknown interaction between activity and Ephexin5-dependent UBE3A synapses. Taken together, our data indicate that removal of Ephexin5 in AS mice functionally restores excitatory synapses in the CA1 to levels similar to those observed in WT animals.

Removal of UBE3A leads to an activity-dependent increase in spine formation that requires Ephexin5.

Why does loss of UBE3A lead to an increase in spine density in an Ephexin5-dependent manner? We hypothesized that altered activity may be the cause due to the hyperactivity of AS neurons[10,30,38,39]; increased firing frequency[25] combined with Ephexin5 being responsive to activity[12,34,40]. To address this mechanistic question, we used primary neuronal cultures. Primary hippocampal neurons were co-transfected with plasmids expressing a UBE3A shRNA (or scrambled shRNA) and plasmids expressing GFP, which has been shown to increase Ephexin5[12]. Neurons were then fixed three days post transfection for confocal imaging. We confirmed the knockdown of UBE3A using immunocytochemistry to show neurons with co-transfected GFP have decreased UBE3A staining as indicated by the arrows (Fig. 5A). Consistent with previous publications, acute cell-autonomous knockdown of UBE3A did not alter baseline spine density within three days post transfection[41].

Previous reports identified decreased synapse density in the CA3 of AS mice[41], which could lead to reduced input onto CA1 neurons. Given the cell autonomous nature of our in vitro UBE3A knockdown, the transfected cells should in theory receive normal input from surrounding WT neurons. To more closely mimic an in vivo AS setting, we cultured hippocampal neurons from WT mice and co-transfected plasmids expressing a UBE3A shRNA or Control shRNA along with a plasmid expressing the G$_i$-associated DREADD (hM4Di)[42] and a plasmid
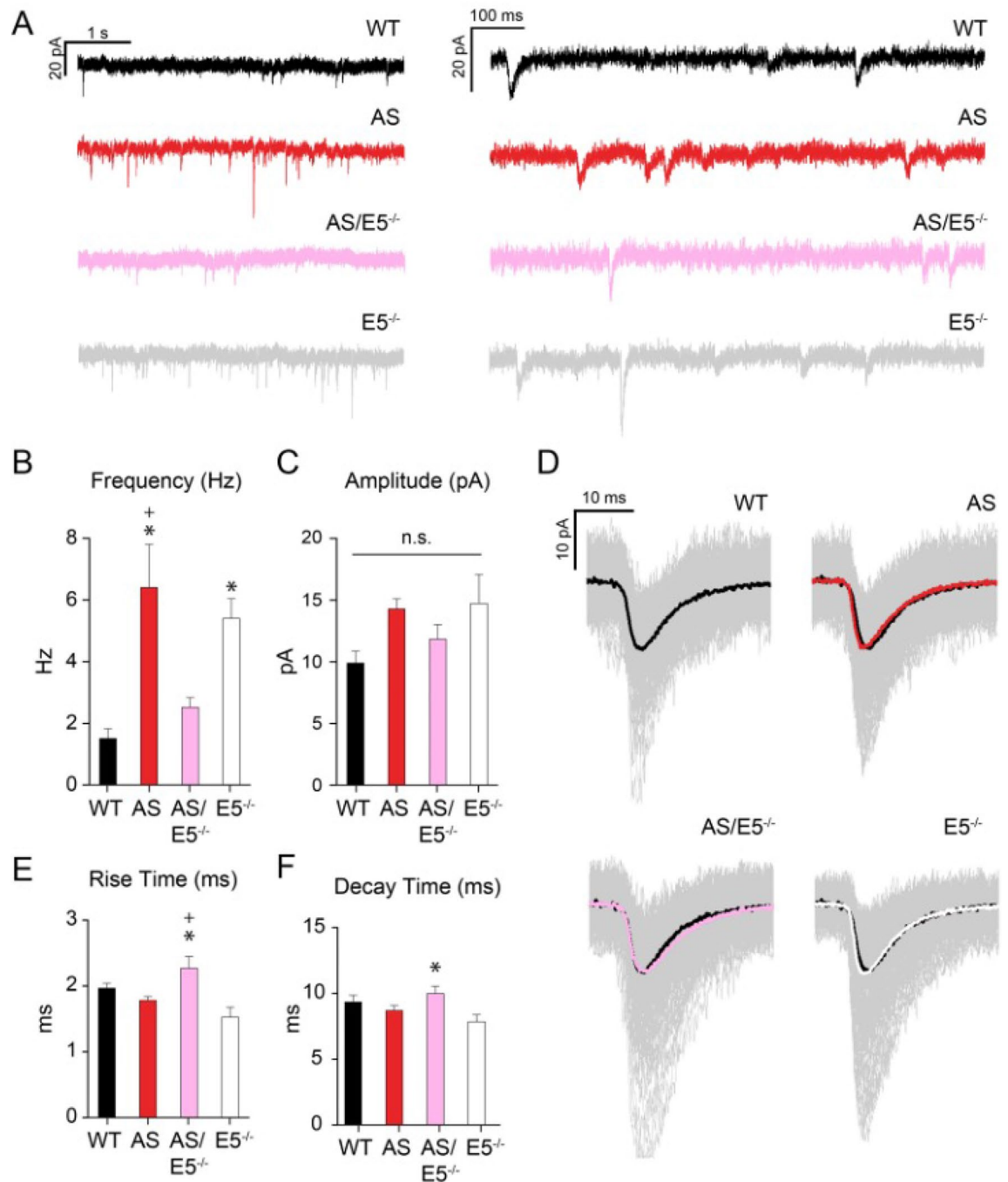
Figure 4. mEPSC frequency, but not amplitude, is altered in the AS CA1 region, and corrected with removal of Ephexin5. (**A**) Representative traces from voltage-clamp recording of each genotype are shown in two different time scales. (**B**) mEPSC frequency recorded from CA1 pyramidal cells represented in Hz. Data are presented as mean ± SEM. *$p < 0.05$ compared to WT and +$p < 0.05$ compared to AS/E5$^{-/-}$ (one-way ANOVA) with *post-hoc* Tukey's multiple comparisons test. (**C**) mEPSC amplitude recorded from CA1 pyramidal cells represented in pA. Data are presented as mean ± SEM. Statistically significant difference between samples was not observed (one-way ANOVA) with *post-hoc* Tukey's multiple comparisons test. (**D**) Representative mEPSC traces for each genotype (average trace in color overlay; individual traces in gray). WT is shown in black in the other genotype traces for comparison. (**E**) Average rise time for individual cells is shown. Data are presented as mean ± SEM. *$p < 0.05$ compared to E5$^{-/-}$, +$p < 0.05$ compared to AS (one-way ANOVA) with *post-hoc* Tukey's multiple comparisons test. (**F**) Average decay times for individual cells are shown. Data are presented as mean ± SEM. *$p < 0.05$ compared to E5$^{-/-}$ (one-way ANOVA) with *post-hoc* Tukey's multiple comparisons test. See also Supplementary Fig. 4. Sample size (n) reported in Materials and Methods. Degrees of freedom and exact *p* values are reported in Supplementary Table 2 and Supplementary Table 3. Analysis was done with MiniAnalysis program (v 6.0—http://www.synaptosoft.com/MiniAnalysis/) and pCLAMP11 (v 10.3.1.4 http://www.molec ulardevices.com).
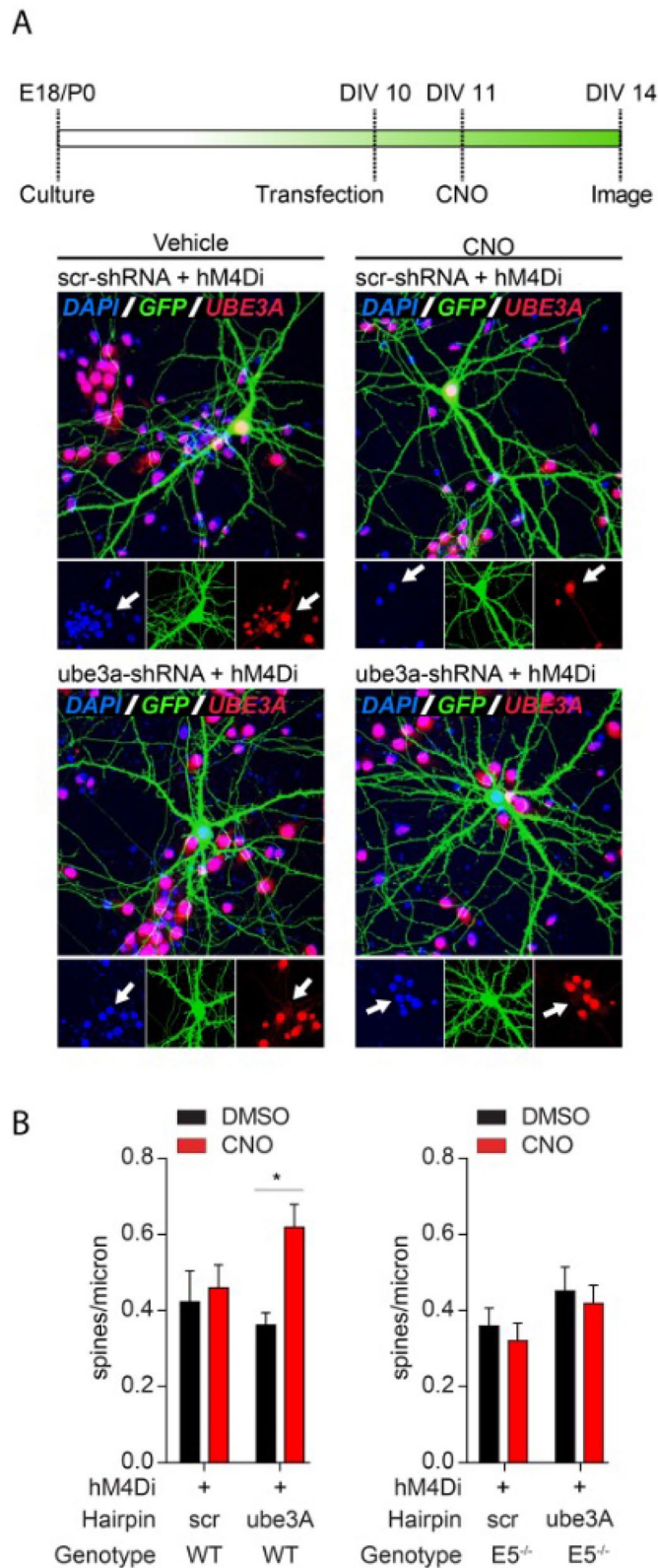
Figure 5. Knockdown of UBE3A leads to an activity dependent increase in dendritic spine formation that requires Ephexin5. (**A**) Hippocampal neuronal cultures were transfected at DIV 10 with plasmids containing GFP, an shRNA hairpin, and hM4Di, and treated with CNO or vehicle from DIV 11–14. Representative neurons at DIV 14 are shown, with white arrows indicating the soma of the transfected cells. Cells were stained for UBE3A (red) and GFP (green). Nuclei were labeled with Hoescht. (**B**) For each treatment group, spine density is shown as spines per micron across the entire transfected neuron. Data are presented as mean ± SEM (n = 3 for all genotypes). *$p < 0.05$ (two-way ANOVA) within genotype with *post-hoc* Sidak's multiple comparisons test. Exact *p* values are reported Supplementary Table 2 and Supplementary Table 3.

expressing GFP. This approach gave us the ability to cell-autonomously remove UBE3A expression and use the DREADD ligand clozapine N-oxide (CNO) to reduce electrical activity within these neurons as a proxy for reduced excitatory inputs. In transfected neurons, knockdown of UBE3A expression combined with CNO treatment lead to a significant increase in spine density (Fig. 5B). Control shRNA treated neurons were unaffected by CNO treatment. Consistent with our hypothesized role for Ephexin5 in UBE3A-dependent spine regulation, the same manipulation in Ephexin5 knockout primary hippocampal neurons did not lead to increased spine density. From these results, we conclude that hippocampal neurons devoid of UBE3A display aberrant activity-dependent regulation of dendritic spine density, which requires the presence of Ephexin5. While these results are not straight forward, they are in line with previous work showing no significant alteration in synapse density under conditions in which activity is higher[38] which is the inverse of our manipulation. Therefore, the relationship between UBE3A-dependent synapse restriction is likely a nuanced and complex interplay between activity and substrate interaction. Although many more questions remain, we believe that these data provide a clue into how loss of UBE3A and dysregulation of at least one substrate may change communication within hippocampal circuits.

Discussion

In the present study, we identify Ephexin5 can be ubiquitylated by UBE3A. These findings provide further support for Ephexin5 being a substrate of UBE3A. Removing Ephexin5 from AS mice restores the cellular and electrophysiological deficits observed in CA1 of AS mice and rescues performance in hippocampus-dependent learning and memory tasks to WT levels. Phenotypes on various strain backgrounds have been shown to exhibit different results for a given task[16–18], but our results indicate a general rescue of hippocampal-dependent phenotypes but not hippocampal-independent phenotypes in both strains. Furthermore, the learning and memory deficits were recapitulated in animals in which UBE3A was conditionally removed in a subset of excitatory neurons located primarily in the hippocampus. These conditional knockout animals were bred on a C57Bl/6J background and clearly exhibited a deficit in novel place preference, which was also rescued by removal of Ephexin5. Our findings support a role for UBE3A in suppressing Ephexin5 expression in adulthood (or post-development) to allow for normal development of excitatory synapses in the hippocampus.

Our study highlights, in adult AS mice, a previously undescribed elevation in hippocampal dendritic spine density and excitatory transmission. Our data suggest this may come from abnormally elevated Ephexin5 expression which leads to aberrant activity-dependent spine plasticity. Removal of Ephexin5 decreases thin spines, a subset of dendritic spines shown to actually be elevated in AS mouse hippocampus[10]. Although Ephexin5 negatively regulates hippocampal spine formation early in development[12], recent work has indicated that Ephexin5 is also required for regulating activity-dependent spine formation in developing neurons[34]. In AS, it is possible that increased expression of Ephexin5 outside of this critical synaptogenic window could be responsible for an abnormal increase in spine formation in CA1 that is activity-related. Recent studies have reiterated a hyperactivity phenotype in AS neurons, providing further evidence for a novel interplay between activity and substrate-dependent dendritic spine development[38,39]. The increase in decay time in the AS/E5$^{-/-}$ animals hints at a possible increase in GluR2-containing AMPA receptors[43], which are typically upregulated during development[44] and correlate with increased spine maturity and stability[45]. Thus, removing Ephexin5 may be preventing the aberrant activity-related formation of new, immature spines in AS mice.

Although our findings in vitro predict that lowered synaptic input into the CA1 neuron in vivo would lead to higher spine density in the CA1 of AS mice, the precise pattern of activity in vivo causing deficits in CA1 remains unknown. However, previous reports have identified imbalances in excitatory/inhibitory transmission in AS mice, which could be a major contributing factor to the Ephexin5-dependent spine deficits we observed in these mice[30]. Based on our data, UBE3A may control activity-dependent spine formation, keeping spine number in check. UBE3A has predominantly been shown to promote synapse development whereby its removal leads to fewer synapses. Whether these changes are relevant to activity-dependent, UBE3A-mediated control of spines is not known. Moreover, while our data appear unexpected, UBE3A overexpression has been reported to inhibit synapse formation in cortical neurons[46]. Taken together, UBE3A's role in activity-dependent and activity-independent brain development and function may be more nuanced than previously appreciated.

Ephexin5 is a promising candidate to target in future efforts to treat AS. We previously reported that modulation of Ephexin5 can ameliorate learning and memory deficits in Alzheimer's disease (AD)[19,47]. Interestingly, a recent study links loss of UBE3A in AD to elevation of Ephexin5 and disease progression[48]. This study also supports Ephexin5 as a substrate of UBE3A in pathological conditions. Furthermore, the expression profile of Ephexin5 (high in early development, low in late development/adulthood and enriched in adult hippocampus) suggests that attempts to reduce its expression are unlikely to have off-target side effects. The lack of behavioral deficits in the Ephexin5 mice also supports the case for exploring Ephexin5 as a viable therapeutic target.

Our findings provide direct evidence in support of a 'UBE3A-substrate hypothesis' of cognitive dysfunction in AS and suggest that modulating these UBE3A-directed substrates can improve UBE3A-related cognitive phenotypes. The specificity of phenotypes that were rescued by removal of Ephexin5 in both the Ube3A$^{loxp-m+/}$ $^{Cre+}$ and UBE3A$^{m-/p+}$ models highlights the importance of identifying additional substrates that could be critical for region-specific UBE3A phenotypes. Notably, removing Ephexin5 did not rescue motor and other non-hippocampus dependent phenotypes. Furthermore, given the strong temporal regulation of Ephexin5 expression, the timing of substrate-directed interventions will likely be important to consider when thinking about distinct AS-related behaviors[49]. In addition to AS research, such efforts to better understand UBE3A substrates may also be relevant for autistic spectrum disorders (ASD), as duplication of the 15q11-13 chromosomal region encompassing the *UBE3A* locus is one of the few characterized persistent cytogenetic abnormalities associated with ASDs, occurring in >1–2% of all ASD cases[50,51].

Materials and methods

(See Supplementary Table 1 for detailed key resources).We have included the N, statistical F scores, and df for individual experiments to provide relevant information when discussing the experimental parameters.

Mice. All animals were socially housed, with food ad libitum on a 14:10 h light/dark cycle. Ephexin5^{+/−} males were crossed with Ube3A[m+/p-]/Ephexin5^{+/−} females to obtain animals that were Ube3A wild type or maternally-deficient and Ephexin5 wild type or null. These crosses were performed in isogenic strains for both 129S7 and C57Bl/6J that had been backcrossed 10 generations, given previous published evidence that a single genetic background in these animals may not be sufficient for determining all phenotypes[16]. To label neurons fluorescently for spine analysis, 129S7 Ube3A[m+/p-]/Ephexin5^{+/−} were crossed with Thy1-EGFP mice (Jackson STOCK Tg(Thy1-EGFP)MJrs/J, 007788), a C57Bl/6J strain, allowing the use of an F1 generation as previously published[16,52]. From this cross, Ephexin5^{+/−} males were crossed with Ube3A[m+/p-]/Ephexin5^{+/−} females, with the EGFP present on either the male or female. WT, AS, AS/E5^{−/−}, and E5^{−/−} animals positive for EGFP were used for analysis. C57Bl/6J CamKIIa-Cre mice were obtained, and expression pattern of this line was determined by crossing these animals to a TdTomato reporter line (Cre[+]/TdTomato[+] animals, Fig. 2A). To selectively remove Ube3A expression from excitatory forebrain neurons, the CamKIIa-Cre line was crossed to floxed-Ube3A mice[26]. Ube3A expression was determined by Western blot analysis after experiments (Fig. 2B). Both sexes were used for all experiments and no sex-specific alterations were discovered. The health of the Ephexin5-null animals has been previously published and we, similarly, saw no overt health issues[12,19].

All animal procedures were performed under protocols compliant with and approved by the Institutional Animal Care and Use Committees of The Johns Hopkins University School of Medicine in accordance with National Institutes of Health guidelines. In addition, we followed the ARRIVE guidelines.

Neuronal cultures. For primary mouse neuronal cultures, wild-type C57BL/6J mice or C57BL/6J Ephexin5^{−/−} mice were sacrificed at P0 and dissected. Brains were removed and dissected cortices were then moved into dissociation buffer (0.3% BSA, 12 mM $MgSO_4$, 10 mM HEPES, 0.6% glucose in Hank's Balanced Salt Solution) plus 16.67 U/ml Papain, which was incubated for 30 min at 37 °C. All neurons were mixed together and contain both male and female neuronal tissue. It was challenging to tell the sex of a mouse embryo and there was not enough material to separate out each embryo and still be able to perform the described biochemical studies in this manuscript. Authenticity of neuronal cultures was in part determined by morphology using light microscopy and immunoblotting of lysates from neuronal cultures with well-validated antibodies to neuronal enriched markers. Proteolyzed tissue was rinsed for 5 min twice in 10 mg/ml Trypsin inhibitor. Tissue was then resuspended in Neurobasal and mechanically dissociated into a single-cell suspension. Cells were counted with a hemocytometer and neurons were plated for imaging on glass coverslips within wells of a 24-well plate at a concentration of 200,000 cells/well.

DNA constructs. The following plasmid constructs were gifts from Dr. Bryan Roth: pcDNA5/FRT-HA-hM4D(Gi) was a gift from Dr. Bryan Roth (Addgene plasmid # 45,548 ; http://n2t.net/addgene:45548 ; RRID:Addgene_45548)[42]. UBE3A shRNA and UBE3A scrambled shRNA (sc-shRNA) were previously described[41].

Antibodies. Ephexin5 antibodies, raised in rabbit against a GST-fusion protein containing Ephexin5 amino acids 1-418, were previously described[12]. The following antibodies are commercially available and used according to manufacturer's suggestions for immunoblotting immunofluorescence studies: UBE3A (Sigma-Aldrich E8655) for Western, UBE3A (Sigma-Aldrich 3E5) for IF, β-Actin (Abcam ab8226), GFP (Aves 1020). Secondary antibodies are described below.

Immunoblotting. For immunoblot analysis, antibodies to Ephexin5 (1:1000, 5% non-fat milk, TBS, 0.05% Tween 20), Actin (1:5000, 5% BSA, TBS, 0.05% Tween 20), and UBE3A (1:2000, 5% non-fat milk, TBS, 0.05% Tween 20) were utilized. Anti-mouse IgG and anti-rabbit IgG secondary antibodies (Cell Signaling Technology 7076S and 7074S, respectively) were used for immunoblotting at a concentration of 1:5000 in the same blocking buffer as the primary antibody. Optical density of the immunoblot bands was quantified using ImageJ.

Expression and purification of GST-Ephexin5. For the generation of purified full-length Ephexin5 protein, a pGEX plasmid encoding N-terminally fused GST-Ephexin5 was transformed into Rosetta DE3 BL21 bacteria. Starter cultures harboring Ephexin5 plasmid were grown overnight at 37 °C and used to inoculate larger cultures the following day at 1:100. Cultures were grown at 37 °C until reaching an OD (600) of 0.6–0.8, at which point cultures were divided into 100 mL volumes and grown at 16 °C for 1 h. GST-Ephexin5 expression was induced by addition of 0.5 μM Isopropyl β-D-1-thiogalactopyranoside and cultures were grown overnight at 16 °C. Cells were spun and harvested in 2.3 M sucrose, 50 mM Tris pH 7.5, and 1 mM EDTA. Recovered cells were lysed on ice for 1 h in 50 mM Tris pH 7.5, 10 mM KCl, 1 mM EDTA, 2 mM DTT, 1 mM PMSF, and 55 mM lysozyme. Lysates were then treated with 0.1% sodium deoxycholate, 25 mM $MgCl_2$, 0.4 nM DNase I for 15 min and insoluble material was separated from lysate via centrifugation at 4000×g for 30 min at 4 °C. To the supernatant, comprised of bacterial lysate containing overexpressed GST-Ephexin5, Glutathione Sepharose beads were added and incubated under constant rotation at 4 °C for 2–4 h. Beads with bound GST-Ephexin5 protein were then rinsed 4 times with 10 mM HEPES pH 7.5, 1 mM DTT, 300 mM NaCl and once with 10 mM HEPES pH 7.5, 1 mM DTT. Protein was then eluted twice from the beads with 50 mM Tris pH8, 10 mM reduced

glutathione. Elutions were dialyzed into 50 mM HEPES pH 8.0, 200 mM NaCl, 10% glycerol, 1 mM TCEP using Slide-A-Lyzer Dialysis Cassette (Extra Strength) with a 10,000 MW cutoff. Dialyzed protein was aliquoted and stored at -80 °C and aliquots were taken for in vitro ubiquitylation assays.

In Vitro Ubiquitination Reaction. The UBE3A in vitro ubiquitination reactions were prepared with the following components from Boston Biochem: 3 μl 10X reaction buffer (500 mM HEPES, 500 mM NaCl, 10 mM TCEP, pH 8), 50 nM UBE1, 1uM UBE2L3, 1 μM E6AP, 1 μM E6, 50 μM Ubiquitin, 10 mM Mg-ATP, and ~ 0.79 ug GST-Ephexin5. Reactions were prepared according to manufacturer's instructions. Briefly, reactions were incubated at 37 °C for 90 or 180 min. Reactions were stopped using Lammeli Buffer to be run on SDS-PAGE for western blotting or flash frozen to be used for mass spectrometry analysis.

Mass Spec ID of ubiquitylations sites. Following in vitro UBE3A ubiquitylation, Ephexin5 was reduced 5 μM dithiothreitol (DTT) 20 mM ammonium bicarbonate at pH 8.5 at 60 °C for 1 h, and after cooling, alkylated with 10 μM iodoacetomide for 15 min at room temperature in the dark. Reduced and alkylated proteins were digested overnight at 37 °C by adding 1:20 Trypsin/LysC mixture: protein in 20 mM ammonium bicarbonate. Peptides from protein digests were desalted using Oasis HLB uElution solid phase extraction plates (Waters) equilibrated and washed with 0.1% TFA, then eluted with 60% acetonitrile in 0.1% TFA and dried by vacuum centrifugation. Desalted peptides were resuspended in 10 μl 2% acetonitrile in 0.1% formic acid and analyzed by reverse phase liquid chromatography coupled to tandem mass spectrometry. Peptides were separated on a pico-frit house packed 75 μm × 200 mm ProntoSIL-120–5-C18 H column (5 μm, 120 Å (BISCHOFF), http://www.bischoff-chrom.com) using 2–90% acetonitrile gradient at 300 nl/min over 90 min on a EasyLC nanoLC 1000 (Thermo Scentific). Eluting peptides were sprayed through 10 μm emitter tip (New Objective, http://www.newobjective.com) at 2.2 kV directly into a Orbitrap Fusion (Thermo Scientific) mass spectrometer. Survey scans (full ms) were acquired from 350–1800 m/z with data dependent isolating the highest number of precursors in a 3 s cycle between each survey scan. Each peptide was isolated with a 1.6 Da window and fragmented with an HCD normalized collision energy of 30 and 15 s dynamic exclusion. Precursor and the fragment ions were analyzed at resolutions 120,000 and 30,000, respectively, with automatic gain control (AGC) target values at 4e5 with 50 ms maximum injection time (IT) and 1e5 with 100 ms maximum IT, respectively. Isotopically resolved masses in precursor (MS) and fragmentation (MS/MS) spectra were extracted from raw MS data without deconvolution and with deconvolution using MS2 Processor in Proteome Discoverer (PD) software. All extracted data were searched using Mascot against the RefSeq2017 protein database with mammalian taxonomy. The following criteria were set for all database searches: sample's species; trypsin as the enzyme, allowing one missed cleavage, and the variable modifications of cysteine carbamidomethylation, Gly-Gly on lysine, methionine oxidation, asparagine and glutamine deamidation. Peptide identifications from Mascot searches were filtered at 1% False Discovery Rate (FDR) confidence threshold, based on a concatenated decoy database search, using Proteome Discoverer. Proteome Discoverer uses only the peptide identifications with the highest Mascot score for the same peptide matched spectrum from the different extraction methods. Mascot results were imported into Scaffold for validation and side-by-side comparisons of MS results.

Behavioral assays. All behavioral testing was done during the animal's dark phase (without a reversed light/dark cycle) with littermate controls when the animals were 11–13 weeks old. The genotypes were blinded to the experimenter during both the tasks and analysis. Animals were habituated to testing room 20 min each day before tasks were begun. Any experiments performed included all 4 genotypes.

Novel place preference. Mice were habituated to the testing arena for 30 min in the testing room. The testing arena was a 10″ × 10″ box with a small visual cue on one side to orient the box. Between each mouse, the arena was cleaned with 70% ethanol. Twenty-four hours later, mice were exposed to 3 different objects for 10 min. An additional twenty-four hours later, mice were placed in the testing arena with the same 3 objects for 10 min, one object having been moved across the arena. Both days with the objects were video recorded. Objects were plastic colored geometric shapes (Learning Resources Mini Geosolids), with each object not repeating color or shape for the individual mouse. A blinded observer scored the amount of time each mouse spent investigating the objects using ODLog (Macropod Software). Investigation was defined as time spent with the mouse's nose within 3 mm of the object, with orientation toward the object. C57Bl/6J WT (n = 11), AS (n = 13), AS/E5$^{-/-}$ (n = 10), E5$^{-/-}$ (n = 11). Object (($F = 2, 123$) = 24.56). Conditional *ube3A^{loxp+}/camkIIa-cre$^+$*: n = 15, Kruskal–Wallis statistic = 2.498; *ube3A^{loxp+}/camkIIa-cre$^-$*: n = 9, F(2, 24) = 0.3827; *ube3A^{loxp+}/camkIIa-cre$^+$/E5$^{-/-}$*: n = 7, F(2, 18) = 12.41; *ube3A^{loxp+}/camkIIa-cre$^-$/E5$^{-/-}$*:n = 12, Kruskal–Wallis statistic 11.07.

Novel object recognition. Similar to Novel Place Preference, except 129S7 mice were exposed to two identical objects. On the third day, instead of moving an object, one of the identical objects was replaced for a unique object. Analysis and timing of experiments is as described above. Mice were excluded before unblinding if they did not investigate the objects during the initial investigation day. This was not restricted to any one genotype with 3–5 animals excluded in WT, AS, and AS/E5$^{-/-}$. 129S7 WT (n = 15), AS (n = 12), AS/E5$^{-/-}$ (n = 18), E5$^{-/-}$ (n = 12). Genotype (df, t ratio): WT (28, 3.22096), AS (22, 1.17592), AS/E5$^{-/-}$ (34, 2.8498), E5$^{-/-}$ (22, 4.9558).

Passive avoidance. C57Bl/6J and 129S7 mice were habituated to the chamber for 15 s before opening of the guillotine door separating the lit chamber from a dark chamber (Coulbourn Instruments). As mice entered the dark chamber, the door closed, mice were shocked (0.3 mA, 2 s) and immediately removed. 24 h later, mice were

placed in the lit box and allowed up to 5 min to enter the shock chamber. Latency on both days was recorded. Both chambers cleaned with 70% ethanol between mice. C57Bl/6J WT (n = 5), AS (n = 6), AS/E5$^{-/-}$ (n = 7), E5$^{-/-}$ (n = 7). Interaction (F (3,42) = 6.349). Day (F (1, 42) = 77.66). Genotype (F(3, 42) = 6.054). 129S7 WT (n = 5), AS (n = 4), AS/E5$^{-/-}$ (n = 4), E5$^{-/-}$ (n = 4). Interaction (F (3,26) = 0.5279). Day (F (1, 26) = 152.8). Genotype (F(3, 26) = 0.5279).

Rotarod. C57Bl/6J and 129S7 mice were habituated to the rotating rod for 10 min at 4 RPM. If animals fell off during this habituation, they were placed back on the rod until the 10 min was complete. After habituation, animals were placed on the rotating rod with increasing speed (4–99 RPM over 5 min) until the animal fell from the rod. The latency to fall was recorded. Each animal was put through 5 trials, with at least 10 min between each trial. For analysis, the highest and lowest latency for each animal was dropped, leaving 3 values per animal. The rotating rod was cleaned with 70% ethanol between each animal. C57Bl/6J WT (n = 10), AS (n = 11), AS/E5$^{-/-}$ (n = 4), E5$^{-/-}$ (n = 5). (F (3,26) = 14.71). 129S7 WT (n = 11), AS (n = 13), AS/E5$^{-/-}$ (n = 14), E5$^{-/-}$ (n = 10). (F (3, 44) = 6.956). Conditional *ube3A^{loxp+}/camkIIa-cre^{+}*: (n = 16), *ube3A^{loxp+}/camkIIa-cre^{-}*: (n = 8). t, df (0.6057, 22).

Marble burying. 16 marbles were evenly spaced in a 10″ × 10″ arena with 2 inches of clean bedding. 129S7 mice were allowed 20 min to freely interact in the arena. Marbles that were completely covered, or covered at least 2/3 in bedding were counted as "buried". Marbles were cleaned with 70% ethanol between each animal use. 129S7 WT (n = 7), AS (n = 8), AS/E5$^{-/-}$ (n = 7) and E5$^{-/-}$ (n = 6). (F (3, 24) = 10.16).

Perfusion and immunofluorescence. For ex vivo immunofluorescence analysis, 8 or 11 week old mice, as indicated, were perfused with ice cold 0.1 M phosphate buffer followed by 4% paraformaldehyde. Brains were removed, post-fixed in 4% paraformaldehyde and 30% sucrose for 4 days before being frozen in Neg50 OCT (Thermo Scientific) 30 micron sections were taken and stored in PBS with sodium azide at 4 °C. Sections were incubated in 5% horse serum in 0.5% Triton-X TBS for 1 h before overnight incubation with 1:500 anti-GFP or 48 h 1:300 anti-UBE3A (3E5 Sigma) and 1 h 1:500 Alexa-Fluor 488 (Thermo Fisher Scientific, A-11039) or Cy3-conjugated (Jackson Immunoresearch, 715–165-151) secondary, respectively. Sections were stained with Hoechst for nuclei labeling before mounting in Fluoromount-G (Southern Biotech).

Ex vivo dendritic spine analysis. Images in a z series projection of three areas of each neuron (basal, proximal and distal) was taken at 63x. To measure spine density, NeuronStudio[53] was used to automatically define neurites and quantify spine number and subtype (thin, mushroom, or stubby) for each neuron image. Per the automated software, thin and mushroom spines were first defined as having a head to neck ratio greater than 1.1. To be further classified as a thin spine if this neck ratio was not met, spines were required to have a length to spine head ratio of 3. Mushroom spines were further defined as having a head diameter of greater than 0.3 μm in addition to the neck ratio of 1.1 or more. Otherwise, spines were classified as stubby. Density was calculated as spines per micron per region per neuron, with multiple neurons per animal. Total (F (3, 32) = 21.38). Oriens (F (3, 32) = 33.59). Radiatum (F (3, 32) = 38.57). Moleculare (F (3, 32) = 21.81).

Electrophysiology recordings. P30 129S7 mice were anesthetized with Euthasol and decapitated. Brains were quickly removed and placed in ice-cold ACSF. Sagittal Sects. (300 μm) containing hippocampus were prepared in ice-cold ACSF using a vibrating blade microtome (Leica VT1200). Right after cutting, slices were recovered for 10 min at 32 °C and then transferred to holding ACSF at room temperature. Cutting and recovery were performed with ACSF containing the sodium substitute NMDG[54]: 92 mM NMDG, 20 mM HEPES (pH 7.35), 25 mM glucose, 30 mM sodium bicarbonate, 1.2 mM sodium phosphate, 2.5 mM potassium chloride, 5 mM sodium ascorbate, 3 mM sodium pyruvate, 2 mM thiourea, 10 mM magnesium, 14 mM sulfate, 0.5 mM calcium chloride. ACSF used for holding slices prior to recording was identical but contained 92 mM sodium chloride instead of NMDG and 1 mM magnesium chloride and 2 mM calcium chloride. ACSF used to perfuse slices during recording contained: 125 mM sodium chloride, 2.5 mM potassium chloride, 1.25 mM sodium phosphate, 1 mM magnesium chloride, 2.4 mM calcium chloride, 26 mM sodium bicarbonate, and 11 mM glucose. All ACSF solutions were saturated with 95% O2 and 5% CO2. For recording, a single slice was transferred to a heated chamber (32 °C) and perfused with normal ACSF (2.5 ml min − 1) using a peristaltic pump (WPI). Visualization of neurons in the pyramidal layer of hippocampal CA1 was performed with an upright microscope equipped for differential interference contrast (DIC) microscopy (BX51WI, Olympus). Whole-cell patch-clamp recordings were made using a MultiClamp 700B amplifier (1 kHz low-pass Bessel filter and 10 kHz digitization) with pClamp 10.3 software (Molecular Devices). Voltage-clamp recordings were made using glass pipets with resistance 3–5 MOhms, filled with internal solution containing: 117 mM cesium methanesulfonate, 20 mM HEPES, 0.4 mM EGTA, 2.8 mM NaCl, 5 TEA-Cl, 2.5 mM Mg-ATP, and 0.25 mM Na-GTP, pH 7.2–7.3 and 285 mOsm. Input resistance was continually monitored on-line; cells with input resistance changes greater than 20% were not included in the analysis. mEPSCs were pharmacologically isolated by having tetrodotoxin (1 μM), gabazine (1 μM), and APV (50 μM) present throughout the experiment and sampled at 1.8 kHz while clamping the cells at − 70 mV. 200–300 events per cell were analyzed, using a threshold of 2X the baseline noise. Analysis of mEPSCs was performed off-line using the MiniAnalysis program (v 6.0). For evoked EPSC experiments, electrical stimuli were delivered in the presence of gabazine (1 μM) to the Schaffer collaterals (stratum radiatum of CA1) at 0.1 Hz via a bipolar electrode. Paired pulse ratios were acquired at -70 mV, by having a second afferent stimulus of equal intensity at several intervals (20–500 ms) after the initial stimulus. The ratio was calculated by dividing the peak amplitude of the second stimulus with the peak amplitude of the first stimulus. Input output curves were obtained by delivering stimuli at a range of intensities (20–500 μAmp) to each cell and measuring

peak amplitudes of evoked EPSCs. For mEPSC frequency and amplitude and rise and decay times, number of cells 129S7: WT (n = 10), AS (n = 13), AS/E5$^{-/-}$ (n = 12), E5$^{-/-}$ (n = 9). Frequency (F(3, 40) = 6.779). Amplitude (F(3, 40) = 2.757). Rise time (F (3, 40) = 6.127. Decay time F (3, 40) = 3.337. For I/O and PPF, number of cells 129S7: WT (n = 14), AS (n = 12). I/O Interaction (F (9, 238) = 2.731), Stimulus Intensity (F (9,238) = 36.46). Genotype (F (1, 238) = 29.93). PPF Interaction (F (4, 118) = 0.9733), Interstimulus Interval (F (4, 118) = 44.34), Genotype (F (1, 118) = 0.6969). 129S7: I/O: WT (n = 11), AS/E5$^{-/-}$ (n = 12). Interaction (F (9, 210) = 1.753), Stimulus Intensity (F (9, 210) = 22.10). Genotype (F (1, 210) = 22.34). PPF: WT n = 10), AS/E5$^{-/-}$ (n = 12). Interaction (F (4, 100) = 0.3177), Interstimulus Interval (F (4, 100) = 27.36), Genotype (F (1, 100) = 2.535).

Transfection. At DIV10, neurons were transfected with plasmids containing GFP to visualize dendritic processes and spines, shRNA hairpin to UBE3A or a scrambled version to knockdown the indicated protein, or HM4D(G$_i$), to modulate activity, using Lipofectamine 2000. In short, the media on the neurons was reduced and media containing a mixture of Lipofectamine 2000 and the plasmid DNA was added for 1 h. The media was completely removed and replaced with the previously removed media.

DREADD drug treatment. At DIV11, neurons were treated with a final concentration of 10 µM CNO dissolved in DMSO or equivalent amounts of DMSO directly into the media. This concentration was maintained through feedings until coverslips were taken for fixing and staining.

Immunocytochemistry. Coverslips were paraformaldehyde fixed in PBS before 48 h incubation in 1:300 mouse anti-UBE3A and 1:300 chicken anti-GFP followed by 1 h 1:500 Cy3-conjugated anti-mouse secondary and 1:500 488-conjugated anti-chicken secondary. Neurons were incubated with Hoechst for nuclei labeling before mounting in Fluoromount-G.

In vitro spine imaging. Images in a z series projection of single neurons were taken at 40× and averaged over 2 images. To measure spine density, NeuronStudio[53] was used to automatically define neurites and quantify spine number for each neuron image. Density was calculated as spines per micron.

Quantification and statistical analysis. Statistical analysis was performed using Graphpad Prism 6. All tests were two-tailed and p values ≤ 0.05 were considered significant. N for each experiment, degrees of freedom, and f/t values are listed in figures or materials and methods. Statistical tests and p values for indicated figures and post-hoc tests and p values for indicated figures are shown in Supplementary Table 2 and Supplementary Table 3.

References

1. Bird, L. M. Angelman syndrome: review of clinical and molecular aspects. *Appl. Clin. Genet.* **7**, 93–104 (2014).
2. Williams, C. A. Neurological aspects of the Angelman syndrome. *Brain Dev.* **27**, 88–94 (2005).
3. Kishino, T., Lalande, M. & Wagstaff, J. UBE3A/E6-AP mutations cause Angelman syndrome. *Nat. Genet.* **15**, 70–73 (1997).
4. Clayton-Smith, J. & Laan, L. Angelman syndrome: A review of the clinical and genetic aspects. *J. Med. Genet.* **40**, 87–95 (2003).
5. Albrecht, U. *et al.* Imprinted expression of the murine Angelman syndrome gene, Ube3a, in hippocampal and Purkinje neurons. *Nat. Genet.* **17**, 75–78 (1997).
6. Jiang, Y. H. *et al.* Mutation of the Angelman ubiquitin ligase in mice causes increased cytoplasmic p53 and deficits of contextual learning and long-term potentiation. *Neuron* **21**, 799–811 (1998).
7. Cooper, E. M., Hudson, A. W., Amos, J., Wagstaff, J. & Howley, P. M. Biochemical analysis of Angelman syndrome-associated mutations in the E3 ubiquitin ligase E6-associated protein. *J. Biol. Chem.* **279**, 41208–41217 (2004).
8. Matentzoglu, K. & Scheffner, M. Ubiquitin ligase E6-AP and its role in human disease. *Biochem. Soc. Trans.* **36**, 797–801 (2008).
9. Yi, J. J. & Ehlers, M. D. Ubiquitin and protein turnover in synapse function. *Neuron* **47**, 629–632 (2005).
10. Wang, J. *et al.* UBE3A-mediated PTPA ubiquitination and degradation regulate PP2A activity and dendritic spine morphology. *Proc. Natl. Acad. Sci. USA* **116**, 12500–12505 (2019).
11. Burette, A. C. *et al.* Subcellular organization of UBE3A in neurons. *J. Comput. Neurol.* **525**, 233–251 (2017).
12. Margolis, S. S. *et al.* EphB-mediated degradation of the RhoA GEF Ephexin5 relieves a developmental brake on excitatory synapse formation. *Cell* **143**, 442–455 (2010).
13. Sailer, C. *et al.* Structural dynamics of the E6AP/UBE3A-E6-p53 enzyme-substrate complex. *Nat. Commun.* **9**, 4441 (2018).
14. Drews, C. M., Brimer, N. & Vande Pol, S. B. Multiple regions of E6AP (UBE3A) contribute to interaction with papillomavirus E6 proteins and the activation of ubiquitin ligase activity. *PLoS Pathog* **16**, e1008295 (2020).
15. Barker, G. R. & Warburton, E. C. When is the hippocampus involved in recognition memory?. *J. Neurosci.* **31**, 10721–10731 (2011).
16. Sittig, L. J. *et al.* Genetic background limits generalizability of genotype-phenotype relationships. *Neuron* **91**, 1253–1259 (2016).
17. Born, H. A. *et al.* Strain-dependence of the Angelman Syndrome phenotypes in Ube3a maternal deficiency mice. *Sci. Rep.* **7**, 8451 (2017).
18. Huang, H. S. *et al.* Behavioral deficits in an Angelman syndrome model: effects of genetic background and age. *Behav. Brain Res.* **243**, 79–90 (2013).
19. Sell, G. L., Schaffer, T. B. & Margolis, S. S. Reducing expression of synapse-restricting protein Ephexin5 ameliorates Alzheimer's-like impairment in mice. *J. Clin. Invest.* **127**, 1646–1650 (2017).
20. Stackman, R. W. Jr., Cohen, S. J., Lora, J. C. & Rios, L. M. Temporary inactivation reveals that the CA1 region of the mouse dorsal hippocampus plays an equivalent role in the retrieval of long-term object memory and spatial memory. *Neurobiol. Learn Mem.* **133**, 118–128 (2016).
21. van der Poel, A. M. Ethological study of the behaviour of the albino rat in a passive-avoidance test. *Acta Physiol. Pharmacol. Neerl.* **14**, 503–505 (1967).

22. Koyavski, L. *et al.* Sex-dependent sensory phenotypes and related transcriptomic expression profiles are differentially affected by Angelman Syndrome. *Mol. Neurobiol.* **56**, 5998–6016 (2019).

23. Dutta, R. & Crawley, J. N. Behavioral evaluation of Angelman syndrome mice at older ages. *Neuroscience* **445**, 163–171 (2020).

24. Cruz, E. *et al.* CIM6P/IGF-2 receptor ligands reverse deficits in Angelman syndrome model mice. *Autism Res.* **14**, 29–45 (2021).

25. Rayi, P. R., Koyavski, L., Chakraborty, D., Bagrov, A. & Kaphzan, H. Alpha1-Na/K-ATPase inhibition rescues aberrant dendritic calcium dynamics and memory deficits in the hippocampus of an Angelman syndrome mouse model. *Prog. Neurobiol.* **182**, 101676 (2019).

26. Judson, M. C. *et al.* GABAergic neuron-specific loss of Ube3a causes Angelman syndrome-Like EEG abnormalities and enhances seizure susceptibility. *Neuron* **90**, 56–69 (2016).

27. McGill, B. E. *et al.* Abnormal microglia and enhanced inflammation-related gene transcription in mice with conditional deletion of Ctcf in Camk2a-Cre-expressing neurons. *J. Neurosci.* **38**, 200–219 (2018).

28. Bruinsma, C. F. *et al.* Dissociation of locomotor and cerebellar deficits in a murine Angelman syndrome model. *J. Clin. Invest.* **125**, 4305–4315 (2015).

29. Hayrapetyan, V. *et al.* Region-specific impairments in striatal synaptic transmission and impaired instrumental learning in a mouse model of Angelman syndrome. *Eur. J. Neurosci.* **39**, 1018–1025 (2014).

30. Wallace, M. L., Burette, A. C., Weinberg, R. J & Philpot, B. D. Maternal loss of Ube3a produces an excitatory/inhibitory imbalance through neuron type-specific synaptic defects. *Neuron* **74**, 793–800 (2012).

31. Kim, H., Kunz, P. A., Mooney, R., Philpot, B. D. & Smith, S. L. Maternal loss of Ube3a impairs experience-driven dendritic spine maintenance in the developing visual cortex. *J. Neurosci.* **36**, 4888–4894 (2016).

32. Dindot, S. V., Antalffy, B. A., Bhattacharjee, M. B. & Beaudet, A. L. The Angelman syndrome ubiquitin ligase localizes to the synapse and nucleus, and maternal deficiency results in abnormal dendritic spine morphology. *Hum. Mol. Genet.* **17**, 111–118 (2008).

33. Haettig, J., Sun, Y., Wood, M. A. & Xu, X. Cell-type specific inactivation of hippocampal CA1 disrupts location-dependent object recognition in the mouse. *Learn. Mem.* **20**, 139–146 (2013).

34. Hamilton, A. M. *et al.* A dual role for the RhoGEF Ephexin5 in regulation of dendritic spine outgrowth. *Mol. Cell Neurosci.* **80**, 66–74 (2017).

35. Tonazzini, I. *et al.* The role of ubiquitin ligase E3A in polarized contact guidance and rescue strategies in UBE3A-deficient hippocampal neurons. *Mol. Autism* **10**, 41 (2019).

36. Harris, K. M., Jensen, F. E. & Tsao, B. Three-dimensional structure of dendritic spines and synapses in rat hippocampus (CA1) at postnatal day 15 and adult ages: implications for the maturation of synaptic physiology and long-term potentiation. *J. Neurosci.* **12**, 2685–2705 (1992).

37. Hering, H. & Sheng, M. Dendritic spines: Structure, dynamics and regulation. *Nat. Rev. Neurosci.* **2**, 880–888 (2001).

38. Sun, A. X. *et al.* Potassium channel dysfunction in human neuronal models of Angelman syndrome. *Science* **366**, 1486–1492 (2019).

39. Avagliano Trezza, R. *et al.* Loss of nuclear UBE3A causes electrophysiological and behavioral deficits in mice and is associated with Angelman syndrome. *Nat. Neurosci.* **22**, 1235–1247 (2019).

40. Schaffer, T.B., Smith, J.E., Cook, E.K., Phan, T. & Margolis, S.S. PKCepsilon inhibits neuronal dendritic spine development through dual phosphorylation of Ephexin5. *Cell Rep.* **25**, 2470–2483 e8 (2018).

41. Greer, P. L. *et al.* The Angelman Syndrome protein Ube3A regulates synapse development by ubiquitinating arc. *Cell* **140**, 704–716 (2010).

42. Armbruster, B. N., Li, X., Pausch, M. H., Herlitze, S. & Roth, B. L. Evolving the lock to fit the key to create a family of G protein-coupled receptors potently activated by an inert ligand. *Proc. Natl. Acad. Sci. USA* **104**, 5163–5168 (2007).

43. Geiger, J. R. *et al.* Relative abundance of subunit mRNAs determines gating and Ca2+ permeability of AMPA receptors in principal neurons and interneurons in rat CNS. *Neuron* **15**, 193–204 (1995).

44. Kumar, S. S., Bacci, A., Kharazia, V. & Huguenard, J. R. A developmental switch of AMPA receptor subunits in neocortical pyramidal neurons. *J. Neurosci.* **22**, 3005–3015 (2002).

45. Suresh, A. & Dunaevsky, A. Relationship between synaptic AMPAR and spine dynamics: Impairments in the FXS mouse. *Cereb. Cortex* **27**, 4244–4256 (2017).

46. Smith, S. E. *et al.* Increased gene dosage of Ube3a results in autism traits and decreased glutamate synaptic transmission in mice. *Sci. Transl. Med.* **3**, 103ra97 (2011).

47. Cook, E. K., Sell, G. L., Schaffer, T. B. & Margolis, S. S. The emergence of Ephexin5 as a therapeutic target in Alzheimer's disease. *Expert Opin. Ther. Targets* **23**, 263–265 (2019).

48. Olabarria, M. *et al.* Dysfunction of the ubiquitin ligase E3A Ube3A/E6-AP contributes to synaptic pathology in Alzheimer's disease. *Commun. Biol.* **2**, 111 (2019).

49. Silva-Santos, S. *et al.* Ube3a reinstatement identifies distinct developmental windows in a murine Angelman syndrome model. *J. Clin. Investig.* **125**, 2069–2076 (2015).

50. Cook, E. H. Jr. *et al.* Autism or atypical autism in maternally but not paternally derived proximal 15q duplication. *Am. J. Hum. Genet.* **60**, 928–934 (1997).

51. Glessner, J. T. *et al.* Autism genome-wide copy number variation reveals ubiquitin and neuronal genes. *Nature* **459**, 569–573 (2009).

52. Copping, N. A. *et al.* Neuronal overexpression of Ube3a isoform 2 causes behavioral impairments and neuroanatomical pathology relevant to 15q11.2–q13.3 duplication syndrome. *Hum. Mol. Genet* **26**, 3995–4010 (2017).

53. Rodriguez, A., Ehlenberger, D. B., Dickstein, D. L., Hof, P. R. & Wearne, S. L. Automated three-dimensional detection and shape classification of dendritic spines from fluorescence microscopy images. *PLoS ONE* **3**, e1997 (2008).

54. Ting, J. T., Daigle, T. L., Chen, Q. & Feng, G. Acute brain slice methods for adult and aging animals: application of targeted patch clamp analysis and optogenetics. *Methods Mol. Biol.* **1183**, 221–242 (2014).

Acknowledgements

Author contributions

G.L.S. and S.S.M. designed experiments. G.L.S., with help from E.K.C., M.A.Z., and T.B.S, performed all behavioral, cellular, and biochemical experiments. R.N.O. and R.N.C. performed mass spectrometry analysis. W.X. performed all electrophysiological recordings. G.L.S., W.X., and E.K.C. were always blind to all genotypes prior to any experimentation and quantification. T.B.S. and S.S.M. blinded experiments. E.K.C. designed and performed all biochemical ubiquitylation assays. G.L.S., W.X., E.K.C., and S.S.M. analyzed and interpreted the data and wrote the paper.

Competing interests

The authors declare no competing interests.

Additional information

Supplementary Information The online version contains supplementary material available at https://doi.org/10.1038/s41598-021-97898-w.

Correspondence and requests for materials should be addressed to G.L.S. or S.S.M.

Reprints and permissions information is available at www.nature.com/reprints.

Publisher's note Springer Nature remains neutral with regard to jurisdictional claims in published maps and institutional affiliations.